JOURNAL OF Applied Polymer SCIENCE

Carbon/Polymer Composite Counter-Electrode Application in Dye-Sensitized Solar Cells

Xueni Zhang, Jing Zhang, Yanzheng Cui, Jiangwei Feng, Yuejin Zhu
Department of Physics, Ningbo University, Ningbo 315211, Zhejiang, China
Correspondence to: J. Zhang (E-mail: zhangjing@nbu.edu.cn) or Y. Zhu (E-mail: zhuyuejin@nbu.edu.cn)

ABSTRACT: Carbon black was embedded in mixtures of poly(ethylene oxide) and poly(vinylidene fluoride–hexafluoropropylene) to make a carbon/polymer composite slurry, which was deposited onto a transparent conducting glass substrate by a doctor-blade coating for application in dye-sensitized solar cells (DSSCs) as a counter-electrode (CE) material. The experiments indicated that the photovoltaic parameters of the DSSCs were strongly dependent on the carbon concentration in the slurry. The device with a carbon CE whose mass ratio was 1 : 1 (mass ratio = carbon black mass to polymer mass) exhibited an overall energy conversion efficiency of 4.62%; this was comparable to that of a device with platinum as a CE (5.32%) under the same test conditions. The better electrocatalytic activity of CE-1.0 (where 1.0 indicates the mass ratio of carbon black to polymer) for the reduction of triiodide resulted a higher performance of the DSSC with such a CE. © 2012 Wiley Periodicals, Inc. J. Appl. Polym. Sci. 000: 000–000, 2012

KEYWORDS: composites; optics; photochemistry

Received 24 April 2012; accepted 4 June 2012; published online
DOI: 10.1002/app.38147

INTRODUCTION

Dye-sensitized solar cells (DSSCs) have attracted much attention because of their low cost, simple fabrication process, and relatively high efficiency of converting light to electricity.[1–6] A typical DSSC consists of three components: a dye-sensitized nanocrystalline titanium dioxide (TiO_2) electrode, a platinum (Pt) counter electrode (CE), and an electrolyte, which usually contains an $I-/I_3^-$ redox couple between the two electrodes. At present, most studies on DSSCs have focused on dye synthesis,[7,8] solid-state (quasi-solid) electrolytes,[9,10] and the theory of electron transport in nanocrystalline titanium films.[11–13] However, there has been much less study on CEs. The CE is one of the most important components in DSSCs; it strongly affects the fill factor (FF) and light-to-electricity of the cells. The task of the CE is the reduction of the redox species used as a mediator in the regeneration of the sensitizer after electron injection or collection of the holes from the hole-conducting material in a solid-state DSSC.

At the moment, several different kinds of CEs have been investigated. Pt-loaded conducting glass has already been widely used as the standard for DSSC CEs because of its good catalytic activity for $I-/I_3^-$ in the electrolyte and its high stability. However, its expensive price and rareness greatly limit its use.[14] Metal substrates, such as steel and nickel, are difficult to employ for liquid-type DSSCs because the $I-/I_3^-$ redox species in the electrolyte are corrosive for these metals. Materials that are abundantly available are preferred when one wants to produce DSSCs on a large scale. Carbon material, such as carbon black, hard carbon spheres, activated carbon, graphite, and carbon nanotubes, with their low cost, high catalytic activity, and good conducting activity, is a promising candidate for the replacement of Pt, which have been used for CEs of DSSCs.

Imoto et al.[15] used activated-carbon-loaded conducting glass as a CE; the energy conversion efficiency of the device was 3.89%, compared to 4.3% for one with a Pt electrode under the same test conditions. Suzuki et al.[16] used single-walled carbon nanotubes for the CE; they were also deposited onto fluorine-doped tin oxide (FTO)–glass and achieved conversion efficiency of 3.5%, compared to 5.4% for one with a Pt electrode under the same test conditions. The carbon film (that Imoto et al. reported) was sintered at a higher temperature on FTO glasses, so it is only suitable for DSSCs with vitreous substrates and could not be used for soft templates. We used composites of carbon and polymer fabricated at low temperature as a CE for DSSCs that could be applied to glass or soft substrates. A soft CE is easily bent so that its shape can be controlled. A flexible CE is suitably chosen according to the particular application of the DSSCs. Furthermore, our experiment obtained a relatively preferable photovoltaic efficiency of 4.62%, compared to 5.32% of the Pt CE.

EXPERIMENTAL

Chemicals and materials

In our experiments, commercial TiO_2 (P25, 20–30 nm, Degussa AG, Germany) was used for the photoelectrode. The sensitizer was bis(tertrabutyl ammonium)-*cis*-bis(thiocynato)bis(2,2′-bipyridy1–4,4′-dicarboxylic acid)–Ru(II) dye (N719, ChemSolarism Chemical Co., Ltd., Suzhou, China). The electrolyte contained iodine (I_2; 99.8%, Beijing, China), 1-butyl-3-methylimidazolium iodide, 4-*tert*-butylpyridine, and guanidine. The polymers in the composites of carbon and polymer CE consisted of poly(ethylene oxide) [weight-average molecular weight (M_w) = 2 × 106 g/mol, Aldrich], poly(vinylidene fluoride–hexafluoropropylene) [P(VDF–HFP); M_w = 4.77 × 10^5 g/mol, Kynar 2801, Elf Atochem, North America]. All other chemicals were analytical grade and included propylene carbonate (99.9%, SCRC, China), 1,2-dimethoxyethane (99.0%, SCRC, China), and $H_2NCH_2{\cdot}CH_2{\cdot}CH_2{\cdot}Si(OC_2H_5)_3$ (WD50, Wuhan University, Wuhan, China). The transparent conductive oxide was FTO glass (Nippon, Japan, 2.2 mm thickness, 15 Ω/cm^2).

Preparation of the CEs

Propylene carbonate and 1,2-dimethoxyethane (6 g) were used as the solvent to dissolve poly(ethylene oxide) (0.05 g) and P(VDF–HFP) (0.05 g) at 80°C by a magnetic stirring apparatus. After all of the polymers were completely dissolved, carbon black was put into the solution. Then, the silicone coupling agent, WD50 (0.1 g), used as a binder, was put into the slurry to make the polymer film composites adhere better onto the FTO. A series of carbon slurries were prepared by changes in the mass ratio of carbon black to the polymer (0.4 : 1, 0.7 : 1, 1 : 1, and 1.3 : 1, the samples of which are referred to as CE-0.4, CE-0.7, CE-1.0, and CE-1.3, respectively). Finally, we made carbon films on conducting glasses by doctor-blade coating, which were heated in an oven at 100°C for about 12 h.

Fabrication of the DSSCs

The commercial TiO_2 (P25) porous films were deposited onto FTO by doctor-blade coating; this was followed by sintering at 450°C for 30 min. The thickness of the TiO_2 films was about 12 μm. The mesoporous TiO_2 films were preheated at 120°C for 30 min before they were immersed in a solution of the dye (N719) overnight. The compositions of the organic-solvent-based liquid electrolyte were 0.6*M* 1-butyl-3-methylimidazolium iodide, 0.03*M* iodine, 0.5*M* 4-*tert*-butylpyridine, and 0.1*M* guanidine. Electrolytes were dropped onto the dye-anchored TiO_2 films, and then, the CE was clipped firmly with the TiO_2/dye/electrolyte.

Characterization measurements

The morphologies of the carbon films were characterized by scanning electron microscopy (SEM; SU-70, Japan). Electrochemical impedance spectroscopy measurements were performed by an electrochemical workstation (CHI650D, Hangzhou DAHUA Apparatus Manufacturing Co., Hangzhou), which also gave the cyclic voltammograms (CVs) and bulk resistance of the CEs. A functional film characteristic tester (DHFC, Hangzhou DAHUA Apparatus Manufacturing Co., Hangzhou, China) was used to test the square resistance of the CEs. A KLA-Tencor Alpha-Step (IQ3, USA) was used to measure the thicknesses of films. The photocurrent–voltage (*J–V*) curves of the cells were obtained by a Keithley model 2400 digital source meter. The irradiation source was a solar simulator (Newport, USA), which gave an AM 1.5-G illumination on the surface of the solar cells. The incident light intensity (100 mW/cm^2) was calibrated with a standard Si solar cell. A mask with a window of 0.16 cm^2 was also clipped onto the TiO_2 side to define the active area of the cell.

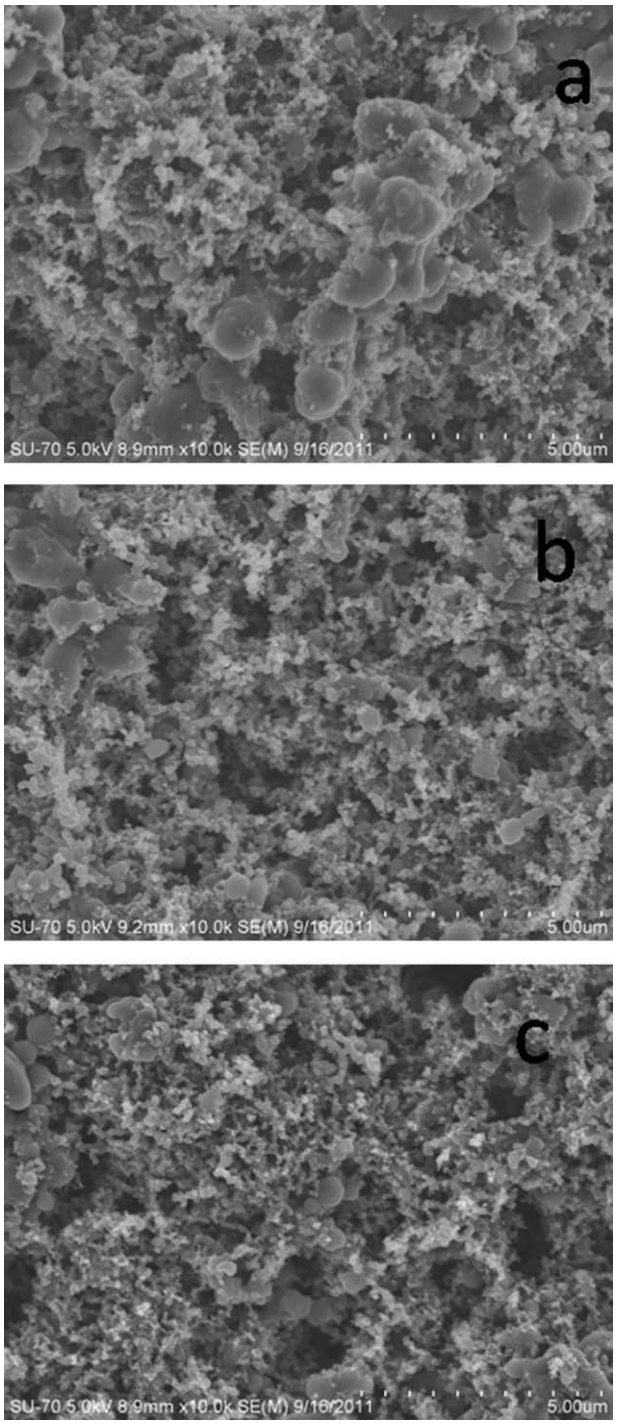

Figure 1. SEM images of the morphologies of the CEs: (a) CE-0.4, (b) CE-1.0, and (c) CE-1.3.

RESULTS AND DISCUSSION

Morphologies of CEs

Figure 1(a–c) depicts the SEM surface morphologies of CE-0.4, CE-1.0, and CE-1.3, respectively. In most filler/polymer

Table I. Sheet Resistance and Bulk Conductivity of the CEs

	CE			
	CE-0.4	CE-0.7	CE-1.0	CE-1.3
Sheet resistance (Ω/cm^2)	551.80	166.92	136.61	94.90
Conductivity (ms/m)	3.02	5.06	6.01	8.10

composites, the ideal morphology is for the filler to be dispersed at nanosize in the polymer matrix. However, in conductive composites, the conductive fillers have to be connected or very close to each other to form conductive paths, as only this kind of structure allows electrons to be transferred from one particle to another.[17] As can be seen in Figure 1, the carbon black nanoparticles, which were dispersed around the polymer molecules, fully penetrated into the polymer matrix. With increasing concentration of carbon black, the carbon black nanoparticles were better connected with each the other so that the electron transportation passes were easily made. As a result, the sheet resistance was played down, and the conductivity was moved up with increasing concentration of carbon black. This was in accordance with experimental results, as can be seen in Table I.

Sheet resistance and bulk conductivity of the CEs

Table I shows the variation of the sheet resistance and bulk conductivity of the CEs with the concentration of slurry. The sheet resistance decreased with the concentration. The bulk conductivity of the CEs was calculated with eq. (1):

$$\sigma = L/(R \times A) \tag{1}$$

where σ is the bulk conductivity of the CEs, L is the thickness of the carbon films, R is the bulk resistance of the CEs, and A is the available area. As shown in Table I, the bulk conductivity of the CEs increased with the concentration of carbon, so the results were in good accordance with previous analyses of the morphologies of the CEs.

CVs of CEs

CV measurements were carried out to evaluate the electrocatalytic activity of the CEs for the reduction of triiodide. Figure 2 shows the CV curves of different CEs in acetonitrile solutions containing 10 m*M* LiI, 10m*M* I_2, or 0.1*M* $LiClO_4$ as the supporting electrolyte; the reference electrode was an AgCl/Ag electrode. As can be seen in Figure 2, the oxidation and reduction peaks of $I-/I_3^-$ for the CEs with different concentrations were almost identical, and they were similar to the Pt CE, which had two pairs redox peaks. The left redox peaks corresponded to eq. (2), and the right ones corresponded to eq. (3):[18]

$$3I^- \leftrightarrow I_3^- + 2e^- \tag{2}$$

$$2I_3^- \leftrightarrow 3I_2 + 2e^- \tag{3}$$

The reduction peak current densities of all of the CEs with different concentrations were slightly higher than that of the Pt CE. This indicated that the CEs were more electrochemically active than the Pt electrode, which manifested a much faster

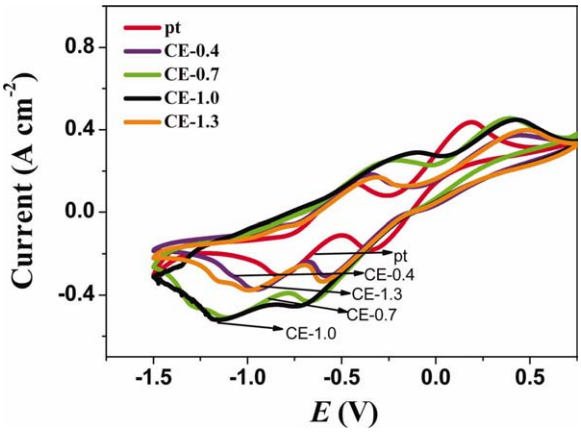

Figure 2. CVs of different CEs at a scan rate of 50 mV/s cycling in electrolyte (10 m*M* LiI + 10 m*M* I_2 + 0.1*M* $LiClO_4$ + acetonitrile). [Color figure can be viewed in the online issue, which is available at wileyonlinelibrary.com.]

reaction rate on the CEs.[19–21] The electrochemical activity of CE-1.0 was the most optimum. All of the DSSCs with CEs showed lower conversion efficiencies than that with a Pt plate, although they showed a higher redox activity. It is known that the Pt plate itself also acts as a light reflector and increases the operation rate of light and could, thus, remarkably improve the efficiency of the solar cells.[2]

Photovoltaic performance of the cells

The *J–V* behavior is a characteristics feature used to determine the photovoltaic performance of solar cells.[22] Figure 3 shows *J–V* curves of the cells based on different CEs. The parameters are summarized in Table II. The FF and overall light-to-electrical energy conversion efficiency (η) values of the DSSCs were calculated according to the following equations:[23]

$$FF = \frac{V_{\max} J_{\max}}{V_{oc} J_{sc}} \tag{4}$$

$$\eta(\%) = \frac{V_{\max} J_{\max}}{P_{in}} \times 100 = \frac{V_{oc} J_{sc} FF}{P_{in}} \times 100 \tag{5}$$

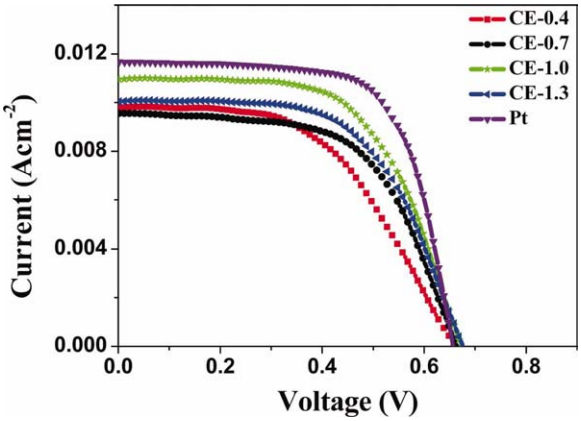

Figure 3. *J–V* curves of the cells based on different CEs. [Color figure can be viewed in the online issue, which is available at wileyonlinelibrary.com.]

Table II. Performance Characteristics of DSSCs Based on Different CEs

CE	V_{oc} (V)	J_{sc} (mA/cm^2)	FF	η (%)
CE-0.4	0.661	9.83	0.532	3.46
CE-0.7	0.663	9.51	0.604	3.81
CE-1.0	0.668	10.94	0.632	4.62
CE-1.3	0.674	10.00	0.626	4.22
Pt	0.656	11.66	0.696	5.32

where J_{sc} is the short-circuit current density (mA/cm^2), V_{oc} is the open-circuit voltage (V), P_{in} is the incident light power, and J_{max} (mA/cm^2) and V_{max} (V) are the current density and voltage at the point of maximum power output on the J–V curves, respectively. It could be seen that the most optimal cell with CEs possessed values of V_{oc} = 0.668 V, J_{sc} = 10.94 mA/cm^2, η = 4.62%, and FF = 0.632. As seen in Tables I and II, despite the sheet resistance of the CEs decreasing with concentration, the photovoltaic performance of the devices based on them was not always better with increasing concentration. An interpretation is given in the following text.

The operation principle of the DSSCs can be described as follows: after the absorption of the photon, the dye molecule became photoexcited and injected an electron into the conduction band of TiO_2. Then, the electron was conducted by a TiO_2 nanoparticle until it reached the conducting SnO_2 back contact. The oxidized-state dye molecule was reduced by iodide in the electrolyte. The produced triiodide diffused to CE, where it was reduced back to iodide by an electron arriving from an external circuit.[24,25] The task of the CE was to transmit electrons from the external circuit. As one of the most important components of the DSSC, the CE strongly influenced the photoelectrochemical performance of the cells.[26] It was clear that the catalytic activity of the CE was crucial for the overall performance of the DSSCs. For example, although CE-1.3 had a lower sheet resistance of about 94.9 Ω/cm^2, when used for a cell, it produced a lower photo to electric energy conversion efficiency and exhibited a lower FF compared to the cell with a CE-1.0 (136.6 Ω/cm^2; Tables I and II). This may have been due to the catalytic activity of CE-1.0 (136.6 Ω/cm^2) being better than that of CE-1.3 (94.9 Ω/cm^2).

Photovoltaic devices are based on the concept of charge separation at an interface of two materials of different conduction mechanisms.[24] The optimal charge separation is responsible for V_{oc} and J_{sc}.[27] For DSSCs, the V_{oc} value generally depends on the difference between the electronic Fermi level (E_f) in the semiconductor and the formal potential of the redox couples (ϕ_{I/I_3^-}) on the CE.[22] It can be calculated by eq. (6):

$$V_{oc} = |E_f - \phi_{I^-/I_3^-}| \quad (6)$$

Because the semiconductor photoelectrodes and the compositions of the electrolytes for all of the solar cells are the same, the V_{oc} value of each photovoltaic device is dependent on the electrochemical properties of the CE. As shown in Figure 3, all of the V_{oc} values of the DSSCs with carbon CEs were slightly higher than those of that with a Pt CE. This was attributed to the higher electrochemical activity of the carbon CEs for redox couples. However, the cells with carbon CEs possessed a relatively low J_{sc}.

Electrochemical impedance spectroscopy of the CEs

Electrochemical impedance spectroscopy was performed to analyze the internal resistance in the DSSCs. Previous analyses have indicated that the internal resistance of solar cells strongly influences the FF and energy conversion efficiency.[28–30] The internal resistances of DSSCs are mainly related to the sheet resistance of the electrodes, the charge-transfer processes occurring at the CEs, the electron transfer at the TiO_2/dye/electrolyte interface, and the carrier transport by ions within the electrolyte.[28,29] There were three semicircles in the electrochemical impedance spectroscopy of the DSSCs. The three semicircles were assigned in order of increasing frequency to the Nernst diffusion impedance of redox species in the electrolyte, the diffusion and recombination of TiO_2 conduction band electrons, and the charge-transfer process at the CE–electrolyte interface.[31] The equivalent circuit for the DSSC is described in Figure 4(a). It consists of the ohmic serial resistance (R_s), three impedance resistances [charge-transfer resistance (R_{ct})], a constant-phase element (Q), and the capacitance (C). Figure 4(b) shows the Nyquist plots of the cells based on CEs with different concentrations, in which the values of R_{ct} could be estimated from the value of the real semicircle. The values of the charge-transfer resistance of the CE–electrolyte interface (R_{ct}^*) are summarized in Table III. The catalytic activity of the electrodes could also be evaluated by the measurement of R_{ct}.[22,32] As can be seen in

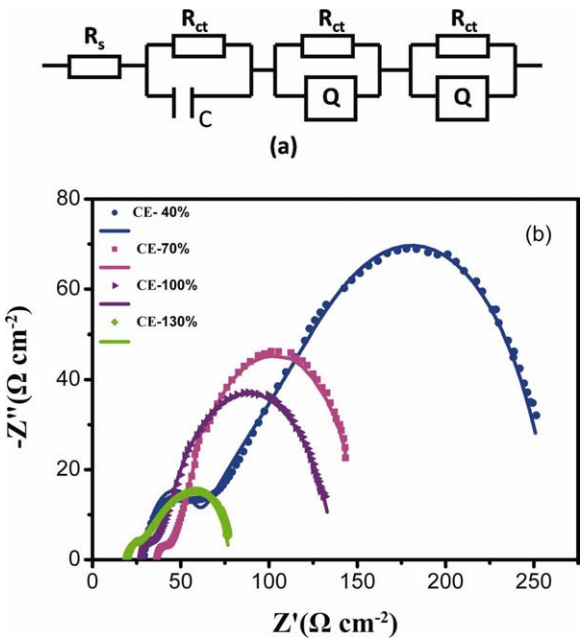

Figure 4. (a) Equivalent circuit for the DSSC based on different CEs, TiO_2/electrolyte interface, and diffusion impedance of redox species in the electrolyte, respectively. (b) Nyquist plots of the cells based on different CEs, the point-formed curves meaning the practical curves, and the lines meaning simulating curves. (Z″ meaning the imaginary part of impedance; Z′ meaning the real part of impedance). [Color figure can be viewed in the online issue, which is available at wileyonlinelibrary.com.]

Table III. Comparison of the R_{ct}^{*} Values for Different CEs

	CE			
	CE-0.4	CE-0.7	CE-1.0	CE-1.3
R_{ct}^{*} (Ω)	29.9	7.1	6.1	9.9

Table III, CE-1.0 possessed the lowest R_{ct}^{*}; hence, it had a relatively higher catalytic activity, so the result of the electrochemical impedance spectroscopy was in good agreement with the CV results. The lowest R_{ct}^{*} of CE (CE-1.0) resulted in minimum series resistance, and hence, the device showed a higher FF and energy conversion efficiency.

CONCLUSIONS

Because carbon materials have a low cost, high catalytic activity, and better conducting activity, a new kind of carbon/polymer composite electrode was fabricated by easy doctor-blade coating in this study. The electrochemical characterizations confirmed that the composite CEs showed better catalytic activity for I_3^- reduction, which led to a high V_{oc}, FF, and final photoelectric conversion efficiency for the fabricated DSSCs. Further investigation revealed relationships between the performances of the carbon/polymer electrodes and the carbon concentrations, the sheet resistance, bulk conductivity, and electrocatalytic activity of CEs. The experiments indicated that the sheet resistance decreased with the concentration and the bulk conductivity of CEs increased with the concentration of carbon. The catalytic activity of the CE had a crucial impact on the photoelectric properties of the DSSCs. The DSSC with CE-1.0 possessed values of V_{oc} = 0.668 V, J_{sc} = 10.94mA/cm^2, FF = 0.632, and η = 4.62%. This accounted accounted for about 86% of the efficiency of the device with a Pt CE. The composite CEs featured an easy fabrication, low cost, and relatively better performance. Therefore, the carbon/polymer composite CEs are viewed as promising CE alternatives for use in low-cost DSSCs.

ACKNOWLEDGMENTS

This work is supported by National Nature Science Foundation of China (contract grant number: 11174163), Science and Technology Innovate Research Team of Zhejiang Province (contract grant number: 2009R50010), and K. C. Wong Magna Fund, Ningbo University.

REFERENCES

1. O'Regan, B.; Grätzel, M. *Nature* **1991,** *353*, 737.
2. Nazeeruddin, M. K.; Kay, A.; Rodicio, I.; Humphry-Baker, R.; Müller, E.; Liska, P.; Vlachopoulos, N.; Grätzel, M. *J. Am. Chem. Soc.* **1993,** *115*, 6382.
3. Frank, A. J.; Kopidakis, N.; Lagemaat, J. V. D. *Coord. Chem. Rev.* **2004,** *248*, 1165.
4. Jayaweera, P. V. V.; Perera, A. G. U.; Tennakone, K. *Inorg. Chim. Acta* **2008,** *361*, 707.
5. Guo, L.; Pan, X.; Zhang, C.; Liu, W.; Wang, M.; Fang, X.; Dai, S. *Sol. Energy* **2010,** *84*, 373.
6. Andrade, L.; Sousa, J.; Ribeiro, H. A.; Mendes, A. *Sol. Energy* **2011,** *85*, 781.
7. Ma, J.; Guo, L. H. *Acta Energiae. Sol. Sinica.* **1995,** *16*, 253.
8. Nazeeruddin, M. K.; Péchy, P.; Renouard, T.; Zakeeruddin, S. M.; Humphry-Baker, R.; Coite, P.; Liska, P.; Cevery, L.; Costa, E.; Shklover, V.; Spiccia, L.; Deacon, G. B.; Biqnozzi, C. A.; Grätzel, M. *J. Am. Chem. Soc.* **2001,** *123*, 1613.
9. Zhang, J.; Han, H. W.; Xu, S.; Wu, S. J.; Zhou, C. H.; Yang, Y.; Zhao, X. Z. *J. Appl. Polym. Sci.* **2008,** *109*, 1369.
10. Li, P. J.; Wu, J. H.; Hao, S. C.; Zhang, L.; Li, Q. H.; Huang, Y. F. *J. Appl. Polym. Sci.* **2010,** *120*, 1752.
11. Lagemaat, J. V. D.; Frank, A. J. *J. Phys. Chem. B* **2001,** *105*, 11194.
12. Duffy, N. W.; Peter, L. M.; Wang, R. L.; Wijayantha, K. G. U. *J. Electroanal. Chem.* **2002,** 524–525, 127.
13. Lin, L.; Lin, J. M.; Wu, J. H.; Hao, S. C.; Lan, Z. *Mater. Res. Innovations* **2010,** *14*, 370.
14. Wei, T. C.; Wan, C. C.; Wang, Y. Y. *Appl. Phys. Lett.* **2006,** *88*, 103122.
15. Imoto, K.; Takahashi, K.; Yamaguchi, T.; Komura, T.; Nakamura, J.; Murata, K. *Sol. Energy Mater. Sol. Cells* **2003,** *79*, 459.
16. Suzuki, K.; Yamaguchi, M.; Kumagai, M.; Yanagida, S. *Chem. Lett.* **2003,** *32*, 28.
17. Yuan, Q.; Wu, D. Y. *J. Appl. Polym. Sci.* **2010,** *115*, 3527.
18. Sun, H. C.; Luo, Y. H.; Zhang, Y. D.; Li, D. M.; Yu, Z. X.; Li, K. X.; Meng, Q. B. *J. Phys. Chem. C* **2010,** *114*, 11673.
19. Lee, K. S.; Lee, H. K.; Wang, D. H.; Park, N. G.; Lee, J. Y.; Park, O. O.; Park, J. H. *Chem. Commun.* **2010,** *46*, 4505.
20. Wang, S. U.; Koteswara Rao, K.; Yang Thomas, C. K.; Wang, H. P. J. *Alloys. Compd.* **2011,** *509*, 1969.
21. Lin, J. Y.; Liao, J. H.; Hung, T. Y. *Electrochem. Commun.* **2011,** *13*, 977.
22. Chen, J. Z.; Li, B.; Zheng, J. F.; Zhao, J. H.; Jing, H. W.; Zhu, Z. P. *Electrochim. Acta* **2011,** *56*, 4624.
23. Grätzel, M. *Prog. Photovoltaics* **2000,** *8*, 171.
24. Grätzel, M. J. *J. Photochem. Photobiol. A* **2004,** *164*, 3.
25. Kong, F. T.; Dai, S. Y.; Wang, K. J. *Adv. Optoelectron.* **2007,** *2007*, 13.
26. Kern, R.; Sastrawan, R.; Ferber, J.; Stangl, R.; Luther, J. *Electrochim. Acta* **2002,** *47*, 4213.
27. Gondek, E.; Kityk, I. V.; Danel, A.; Sanetra, J. *Spectrochim. Acta A* **2008,** *70*, 117.
28. Han, L.; Koide, N.; Chiba, Y.; Islam, A.; Komiya, R.; Fuke, N.; Fukui, A.; Yamanaka, R. *Appl. Phys. Lett.* **2005,** *86*, 1.
29. Koide, N.; Islam, A.; Chiba, Y.; Han, L. Y. *Photochem. Photobiol. A* **2006,** *182*, 296.
30. Hauch, A.; Georg, A. *Electrochim. Acta* **2001,** *46*, 3457.
31. Easwaramoorthi, R.; Chun, J. Y.; Lee, J. W. *Carbon* **2010,** *48*, 4556.
32. Gagliardi, S.; Giorgi, L.; Giorgi, R.; Lisi, N.; Dikonimos Makris, T.; Salernitano, E.; Rufoloni, A. *Superlattices Microstruct.* **2009,** *46*, 205.